

# Radiative cooling in relativistic collisionless shocks. Can simulations and experiments probe relevant GRB physics?

Mikhail V Medvedev<sup>1‡</sup> and Anatoly Spitkovsky<sup>2</sup>

<sup>1</sup> Department of Physics and Astronomy, University of Kansas, KS 66045

<sup>2</sup> Department of Astrophysical Sciences, Peyton Hall, Princeton University,  
Princeton, NJ 08544

E-mail: medvedev@ku.edu

**Abstract.** We address the question of whether numerical particle-in-cell (PIC) simulations and laboratory laser-plasma experiments can (or will be able to, in the near future) model realistic gamma-ray burst (GRB) shocks. For this, we compare the radiative cooling time,  $t_{\text{cool}}$ , of relativistic electrons in the shock magnetic fields to the microscopic dynamical time of collisionless relativistic shocks — the inverse plasma frequency of protons,  $\omega_{pp}^{-1}$ . We obtain that for  $t_{\text{cool}}\omega_{pp}^{-1} \lesssim$  few hundred, the electrons cool efficiently at or near the shock jump and are capable of emitting away a large fraction of the shock energy. Such shocks are well-resolved in existing PIC simulations; therefore, the microscopic structure can be studied in detail. Since most of the emission in such shocks would be coming from the vicinity of the shock, the spectral power of the emitted radiation can be directly obtained from finite-length simulations and compared with observational data. Such radiative shocks correspond to the internal baryon-dominated GRB shocks for the conventional range of ejecta parameters. Fermi acceleration of electrons in such shocks is limited by electron cooling, hence the emitted spectrum should be lacking a non-thermal tail, whereas its peak likely falls in the multi-MeV range. Incidentally, the conditions in internal shocks are almost identical to those in laser-produced plasmas; thus, such GRB-like plasmas can be created and studied in laboratory experiments using the presently available Petawatt-scale laser facilities. An analysis of the external shocks shows that only the highly relativistic shocks, corresponding to the extremely early afterglow phase, can have efficient electron cooling in the shock transition. We emphasize the importance of radiative PIC simulations for further studies.

PACS numbers: 98.70.Rz, 52.72.+v, 52.35.-g, 95.30.Qd, 52.65.Rr

Submitted to: *Astrophys. J.*

## 1. Introduction

It has been shown in recent years that collisionless relativistic shocks are mediated by the Weibel instability — a current filamentation instability that produces strong, sub-equipartition magnetic fields at the shock front (Medvedev & Loeb 1999). This is an attractive model for gamma-ray bursts (GRBs), because it puts a synchrotron shock

‡ Also: Institute for Nuclear Fusion, RRC “Kurchatov Institute”, Moscow 123182, Russia

model on a firm physical ground. However, it has been thought that the generated magnetic fields should occupy an extremely small volume of the shocked region, hence the radiation emitted by the relativistic electrons in these fields should be extremely weak and astrophysically unimportant. Conventionally, one assumes that the strong Weibel fields live on scales of tens of plasma skin depths (tens of  $c/\omega_{pp}$ ) behind the shock, which ranges from only few centimeters in internal shocks to about  $10^8$  cm or so in external shocks; both are some ten orders of magnitude smaller than the typical size of the shocked region. Therefore, unless the synchrotron cooling length,  $t_{\text{cool}}c$ , is comparably small, the radiative efficiency of such shocks should indeed be very small. This further raises a concern that a number of numerical particle-in-cell (PIC) simulations attempting to model GRB shocks<sup>§</sup> (Spitkovsky 2008; Chang *et al* 2008; Keshet *et al* 2008) probe spatial scales that are too small, and, hence, cannot be used to deduce the radiation spectrum of GRB emission. This also can cast some doubt on jitter radiation as a viable explanation of spectral properties of prompt GRBs (Medvedev 2000, 2006; Hededal 2005). Recently, long duration shock simulations (Keshet *et al* 2008) and analytical works (Katz *et al* 2007; Couch *et al* 2008; Sironi & Goodman 2007; Goodman & MacFadyen 2007; Milosavljevic *et al* 2007) have suggested that appreciable magnetic fields could still survive in the downstream region due to the effects of accelerated particles or the field amplification by upstream turbulence. Regardless of the ultimate resolution of the magnetic decay question, there exists another physical regime where most of the radiation is produced near the shock, rather than in its downstream. Simulations of such shocks then capture most of the relevant physics without the need to simulate the far downstream region. In this paper, we explore the relevance of such shocks to GRB scenarios.

We use the results of recent numerical simulations of relativistic collisionless shocks in electron-ion (Spitkovsky 2008) and electron-positron (Chang *et al* 2008; Keshet *et al* 2008) plasmas to estimate and compare the electron cooling and plasma time-scales in the shock transition region. We then deduce the parameter range of internal (both baryon-dominated and electron-positron pair-dominated) and external shocks, for which the shocks can be considered as radiatively efficient, i.e., the radiated energy in the shock transition is of order the electron energy  $\gamma_e m_e c^2$ , where  $\gamma_e$  is an average Lorentz factor of the bulk electrons. We find that internal shocks are in this radiative regime for a reasonable range of model parameters,  $\Gamma \sim 200 - 300$  and  $\Gamma_i \gtrsim 2.5$ , where  $\Gamma$  and  $\Gamma_i$  are, respectively, the bulk Lorentz factor of the ejecta and the Lorentz factor of an internal shock inside the ejecta, measured in the center of mass frame of the colliding shells. In contrast, external shocks may be in the radiative regime only at very early times, less than 100 seconds after the explosion. We also argue that the physical conditions in internal shocks are very close to those that can be achieved in laser-plasma interaction experiments. Therefore, the physics of the Weibel instability and jitter radiation can be studied experimentally at laser-plasma facilities, such as *Omega EP*, *NIF* and others. In particular, the *Hercules* experiment has been proposed and is now under development at the University of Michigan (Reynolds *et al* 2006, 2007; Huntington *et al* 2008; for technical details, see Maksimchuk *et al* 2008) to create and diagnose the Weibel instability and turbulence in the laboratory high-energy density plasmas, as a part of the Laboratory Astrophysics and High-Energy Density Physics programs.

<sup>§</sup> These 2D simulations studying shocks in electron-positron plasma are extending to at most ten thousand skin depths, i.e., of order tens of meters (in the shock co-moving frame) for internal shocks.

## 2. Dimensionless electron cooling time

The electron synchrotron cooling time is obtained from the relation that the emitted energy is of order the initial electron's energy:

$$P_{\text{syn}} t_{\text{cool}} = (4/3) \sigma_T c \gamma_e^2 (B^2/8\pi) t_{\text{cool}} \sim \gamma_e m_e c^2. \quad (1)$$

Here,  $\sigma_T$  is the Thompson cross-section,  $\gamma_e$  is the Lorentz factor of the emitting electron, and  $P_{\text{syn}}$  is the synchrotron emission power per electron. This gives

$$t_{\text{cool}} = \frac{6\pi m_e c}{\sigma_T \gamma_e B^2}. \quad (2)$$

Note that this expression holds for jitter radiation as well, because the total emitted power by an electron in the jitter regime is identical to that of synchrotron (Medvedev 2000).

We will compare  $t_{\text{cool}}$  to the characteristic time of the plasma processes at a shock, the inverse *relativistic* plasma frequency of the protons,  $\omega_{pp}^{-1}$ , which is

$$\omega_{pp} = \left( \frac{4\pi e^2 n'}{\Gamma_i m_p} \right)^{1/2}, \quad (3)$$

where  $n'$  is the particle density behind the internal shock measured in the downstream frame. To within a factor of two, the so-defined  $\omega_{pp}$  corresponds to the nonrelativistic upstream plasma frequency, because  $n' = 4n\Gamma_i$ , where  $n$  is the particle density of the unshocked ejecta in its own co-moving frame. It is natural to introduce the dimensionless cooling time

$$T_{\text{cool}} = t_{\text{cool}} \omega_{pp}. \quad (4)$$

In our analysis we will use the results of electron-ion (Spitkovsky 2008) and electron-positron (Chang *et al* 2008) shock PIC simulations. Apparently, the evolution of currents and magnetic fields in the vicinity of a shock in electron-proton and electron-positron plasmas does not differ substantially, because in the electron-proton case the electrons in the downstream carry about 30% – 50% of the proton energy and, hence, their effective mass is comparable to the proton mass. ||

Figure 1 represents a snapshot of a steady state shock in the electron-ion plasma obtained from a PIC simulation with Lorentz factor  $\Gamma = 15$  and mass ratio  $m_i/m_e = 100$  (Spitkovsky 2008). This and other simulations (Chang *et al* 2008; Keshet *et al* 2008) indicate that the strongest magnetic fields with energy density  $\gtrsim 10\%$  of the kinetic energy density occupy the region of few tens of ion plasma skin-depths around the main shock compression, as measured in the frame of the downstream fluid. Hereafter, we will use the value of  $l \sim 50c/\omega_{pp}$  for the transition length (for electron-positron shocks, the ion plasma frequency is replaced with the plasma frequency of pair plasma). Since the fields are highly inhomogeneous, we assume a factor of two uncertainty in this number. The shock moves at  $v = c/3$  (or  $c/2$  in 2D) in the downstream frame, hence the electron residence time in the region of high field is  $t_{\text{res}} \sim l/v \sim 150\omega_{pp}^{-1}$ . Taking the uncertainty in  $l$  and other parameters into account, we estimate that  $t_{\text{res}} \sim (100 - 300)\omega_{pp}^{-1}$ . We did not account here for

|| One has to be careful here because the parallel and perpendicular relativistic masses are not identical,  $m_{e,\perp} \sim \gamma_e m_e \sim \Gamma_i m_p$  and  $m_{e,\parallel} \sim \gamma_e^3 m_e \sim \Gamma_i m_p (\Gamma_i m_p / m_e)^2 \gg \Gamma_i m_p$ . Hence, the electrons will be effectively much heavier than the protons with respect to their acceleration/deceleration, but should behave similar to the protons with respect to deflection and pitch-angle scattering.

the clumpiness of magnetic inhomogeneities, which shortens the effective  $t_{\text{res}}$ , and the electron trapping in high-field clumps, which is increasing the effective residence time. Interestingly, in the far downstream region, the magnetic energy decreases with the distance  $d$  from the shock as  $\propto d^{-1}$  (Chang *et al* 2008). An electron in this region loses energy logarithmically slowly,  $E \propto \ln(d)$ . If this scaling holds through a large distance downstream, this implies two possibilities. First, if  $t_{\text{cool}} \lesssim t_{\text{res}}$ , then the electrons lose their energy quickly near the shock jump; hence the radiative efficiency of such a shock is high. The electron cooling will substantially affect the structure of the downstream region, in this regime. Second, if  $t_{\text{cool}} \gg t_{\text{res}}$ , then the electrons lose only a small fraction of their energy, which makes this shock radiatively inefficient. Therefore, we refer to a shock as a “radiative shock” if  $T_{\text{cool}} \lesssim 300$  and as a “weakly radiative shock” otherwise. Interestingly, if  $T_{\text{cool}} \lesssim 10 - 50$ , radiative cooling might be substantial already in the upstream region (where the Weibel instability creates current filaments and magnetic fields), before the main shock compression. We expect that the very formation of such a shock may be strongly affected by radiative cooling of electrons. We refer to the regime of  $T_{\text{cool}} \lesssim 10 - 50$  as the “strong cooling regime.”

### 3. Shock models

#### 3.1. Internal shocks in baryon-dominated ejecta

Internal shocks occur inside the ejected material when inhomogeneities, often referred to as “shells” that have different masses and velocities, collide with each other relativistically. Radiation emitted at the internal shocks is thought to be the prompt gamma-ray radiation of a GRB (e.g., Mészáros 2006).

Here we conventionally assume that a central engine produces an ultra-relativistic wind with the kinetic luminosity,  $L \sim 10^{52}$  erg/s and the Lorentz factor  $\Gamma \gtrsim 100$  (Mészáros & Rees 2000; Rees & Mészáros 2005; Pe’er & Waxman 2004). At a radial distance,  $R$ , from the central engine, the co-moving particle density of the ejecta is

$$n = \frac{L}{4\pi R^2 \Gamma^2 m_p c^3} \simeq (1.8 \times 10^{15} \text{ cm}^{-3}) L_{52} R_{12}^{-2} \Gamma_2^{-2}, \quad (5)$$

where we use the convention that  $L_{52} = L/(10^{52} \text{ erg/s})$  and similarly for other quantities, whereas if no numerical subscript is present, then the quantity is in CGS units. The density in the downstream of an internal shock is

$$n' = 4\Gamma_i n. \quad (6)$$

The magnetic field in the downstream and the electron bulk Lorentz factor are calculated as fractions  $\epsilon_B$  and  $\epsilon_e$  of the post-shock thermal energy density,  $U = n'(\gamma_p m_p c^2 + \gamma_e m_e c^2) \sim n' \Gamma_i m_p c^2$  (in the last equality, we neglected the electron contribution, for simplicity, though it may change  $U$  by a factor  $\epsilon_e/[1 + \epsilon_e]$ ),

$$B' = (8\pi \Gamma_i m_p c^2 n' \epsilon_B)^{1/2} \simeq (1.6 \times 10^7 \text{ G}) L_{52}^{1/2} \Gamma_2^{-1} R_{12}^{-1} \epsilon_B^{1/2}. \quad (7)$$

$$\gamma_e = (m_p/m_e) \Gamma_i \epsilon_e \simeq 1.8 \times 10^3 \Gamma_i \epsilon_e. \quad (8)$$

For the parameters  $\epsilon_e$  and  $\epsilon_B$  one has to use the emission-weighted quantities, rather than the conventionally used volume-averaged ones, because fields are highly inhomogeneous in the shock region. This effect is particularly important for  $\epsilon_B$  and less so for  $\epsilon_e$  because high-energy electrons are distributed more or less uniformly. PIC simulations indicate that  $\epsilon_e \sim 0.5$  (electrons carry 50% of the proton energy) and that

$\epsilon_B$  reaches unity locally (Spitkovsky 2008; Chang *et al* 2008). High energy radiation from electrons is not included in the present code. In order to calculate the emission-weighted  $\hat{\epsilon}_e$  and  $\hat{\epsilon}_B$  (black curves in panels (d) and (e) in figure 1, hereafter denoted with a “hat” symbol) we took into account that radiative losses are proportional to  $B^2\gamma_e^2$ . Since the electron cooling occurs predominantly in the high-field regions, a larger effective  $\hat{\epsilon}_B$  and  $\hat{\epsilon}_e$  would be deduced from observations. Taking into account the factor of 8 difference in the definition of  $\epsilon_B$  here and in Spitkovsky 2008; Chang *et al* 2008, we estimate the emission-weighted value as  $\hat{\epsilon}_B \sim 1/8 \sim 0.1$ .

Finally, the dimensionless cooling time in baryon-dominated internal shocks becomes

$$T_{\text{cool}}^{(e^-p)} \simeq 170L_{52}^{-1/2}\Gamma_2\Gamma_i^{-3}R_{12}\hat{\epsilon}_B^{-1}\hat{\epsilon}_e^{-1}. \quad (9)$$

We assume that the shells have different masses but carry similar linear momenta,  $p \sim \Gamma_s m_s c \sim \Gamma_r m_r c$ . That is, in this scenario, a constant driving force is assumed to continuously eject material while the central engine is active. Thus, the variation in the Lorentz factor of the shells is simply reflecting the variation of the density of the ejecta (i.e., that of the shell masses). An attractive feature of this model is that the total energy of the ejecta is uniformly distributed among individual shells, which nicely fits into the relativistic wind picture, unlike the model with shells of equal mass, in which the fastest shell essentially dominates the energetics of the outflow. In the collision of two shells, two shock waves are formed, which propagate through each shell (Kobayashi *et al* 1997). The center of mass Lorentz factor of the two shells is

$$\Gamma_c = \frac{m_s\Gamma_s + m_r\Gamma_r}{[m_s^2 + m_r^2 + m_s m_r (\Gamma_s/\Gamma_r + \Gamma_r/\Gamma_s)]^{1/2}}, \quad (10)$$

so  $\Gamma_c \sim \sqrt{2}\Gamma_s$  for  $\Gamma_s m_s \simeq \Gamma_r m_r$  and  $\Gamma_r \gg \Gamma_s$ . The thermal energy density in the downstream of each shock is related to the Lorentz factor of the shells in their center of mass frame:

$$(\Gamma_i)_{s,r} \simeq (1/2)(\Gamma_{s,r}/\Gamma_c + \Gamma_c/\Gamma_{s,r}), \quad (11)$$

so that the Lorentz factor of an internal shock can be as high as  $\Gamma_i \sim 2^{-3/2}\Gamma_r/\Gamma_s$ , which is at least a few if the Lorentz factors of the “slow” and “rapid” shells are, say,  $\Gamma_s \sim 100$  and  $\Gamma_r \sim 1000$ , respectively, that is  $m_s/m_r \sim 10$ .

We assume that the central engine is an accretion disk around a solar mass black hole. Thus, the flow forms at a few to ten Schwarzschild radii. This sets the variability time scale,  $t_v \sim 10^{-4}$  s. Present observations confirm the variability on a millisecond scale, but are not capable of resolving sub-millisecond time scales. In this model, the relativistic shells are ejected from the radius  $R_0 \sim ct_v$  and their initial separation is of order  $R_0$  as well. A collision of the two shells will occur at the radius

$$R_i \simeq 2R_0 (\Gamma_s^{-2} - \Gamma_r^{-2})^{-1} \sim 2\Gamma_s^2 ct_v \sim (6 \times 10^{10} \text{ cm})\Gamma_2^2 t_{v,-4}. \quad (12)$$

One should keep in mind that collisions of the shells can occur at substantially smaller radii, if the wind modulation occurs due to instabilities in the outflow (e.g., a jet), at radii  $R \gg R_0$  where the flow is already ultra-relativistic (Rees & Mészáros 2005).

Due to the presence of electrons in the baryonic outflow, the co-moving optical depth due to Thompson scattering,  $\tau_b \sim n\sigma_T(R/\Gamma)$ , approaches unity at the radius

$$R_{\text{ph}} = \Gamma/(n\sigma_T) \simeq (1.2 \times 10^{13} \text{ cm})L_{52}\Gamma_2^{-3}, \quad (13)$$

where  $\sigma_T$  is the Thompson cross-section and  $R/\Gamma$  is the co-moving length. For a radiative luminosity of a GRB of  $L_\gamma \sim 0.1L$  (we assumed a 10% radiation efficiency),

the electron-positron pair opacity is obtained from the balance between the rates of annihilation and of pair production. The latter is the photon density above the electron rest mass over the co-moving dynamical time (Pe'er & Waxman 2004). Taking into account that only the photons with energies above  $m_e c^2$  can produce pairs, the pair-producing luminosity is  $L_\gamma^> \simeq (\hbar\nu_{\text{syn}}/m_e c^2)^\beta L_\gamma$  if  $\hbar\nu_{\text{syn}} < m_e c^2$  and  $L_\gamma^> = L_\gamma$  otherwise, where  $\nu_{\text{syn}} = \gamma_e^2 (eB'/m_e c)$  is the co-moving synchrotron frequency,  $\beta \sim 0.5$  is the high-energy spectral slope  $\nu F_\nu \propto \nu^{-\beta}$ . Finally, we obtain the pair optical depth to be equal to the square root of the co-moving compactness,  $\tau_\pm \sim l^{1/2} \sim (L_\gamma^> \sigma_T / 4\pi R \Gamma^3 m_p c^3)^{1/2}$ . The radius of the pair photosphere,  $\tau_\pm \sim 1$ , is

$$R_{\text{pair}} = L_\gamma^> \sigma_T / 4\pi \Gamma^3 m_p c^3 \simeq (2.2 \times 10^3 \text{ cm}) L_{\gamma,51} \Gamma_2^{-3}. \quad (14)$$

In the last expression we omitted the spectral correction, for simplicity. Note that non-thermal spectra can be seen even for relatively large  $\tau_\pm$  of few tens (Pe'er & Waxman 2004). Since the optical depth increases with decreasing radius as  $\tau_\pm \propto l^{1/2} \propto R^{-1/2}$ , one can observe non-thermal spectra produced at internal shocks at radii as small as  $\sim 10^{-3} R_{\text{pair}}$  or so. Note also that the position of the pair photosphere depends on (unknown) radiative efficiency.

Figure 2 shows the regions of strong and weak radiative cooling versus  $R$  and  $\Gamma$  for a reasonable and a rather extreme cases of  $\Gamma_i = 4$  and  $\Gamma_i = 10$ . One can see that internal shocks in the strong cooling regime,  $T_{\text{cool}} \lesssim 10$ , can occur for  $\Gamma \lesssim 10^{2.1} \sim 125$  and at  $R \lesssim \text{few} \times (10^{10} - 10^{11})$ , well below the photosphere at such low  $\Gamma$ 's; hence, radiation from such shocks is hardly observable. Strongly radiative shocks  $T_{\text{cool}} \sim 100 - 300$  can occur above the baryonic photosphere for reasonable values of  $\Gamma \lesssim 200 - 300$  and  $\Gamma_i \gtrsim 2.5$ ; hence they are likely observable. At the photosphere,  $R_{\text{ph}} = R_i$ , we have

$$R_{i,\text{ph}} \simeq (4.9 \times 10^{11} \text{ cm}) L_{52}^{2/5} t_{v,-4}^{3/5}, \quad (15)$$

$$\Gamma(R_{i,\text{ph}}) \simeq 290 L_{52}^{1/5} t_{v,-4}^{-1/5}, \quad (16)$$

which depend weakly on the central engine parameters. Excluding  $R$  and  $\Gamma$  in Eq. (9), we obtain

$$T_{\text{cool}}^{(e^-p)}(R_{i,\text{ph}}) \simeq 250 L_{52}^{1/10} t_{v,-4}^{2/5} \Gamma_i^{-3} \hat{\epsilon}_B^{-1} \hat{\epsilon}_e^{-1}, \quad (17)$$

We plot the the regions of strong and weak cooling versus  $R$  and  $\Gamma_i$  in the left panel of figure 3 and  $T_{\text{cool}}$  vs.  $\Gamma_i$  in right panel. We conclude that internal shocks with  $\Gamma_i$  as low as 2.5 can be radiatively efficient.

The peak of the synchrotron radiation in the observers frame is

$$\nu_{\text{syn}} = (eB/m_e c) \gamma_e^2 \Gamma \simeq 400 \text{ MeV } L_{52}^{1/2} R_{12}^{-1} \Gamma_i^3 \hat{\epsilon}_B^{1/2} \hat{\epsilon}_e^2. \quad (18)$$

If radiation is emitted in the jitter regime, the spectral peak is expected to be a bit higher:  $\nu_j \simeq \nu_{\text{syn}} \sqrt{(m_i/m_e) \hat{\epsilon}_B} \sim 10 \nu_{\text{syn}}$  (Medvedev 2000; Medvedev *et al* 2007). Thus, for the assumed parameters the emission is expected to be peaked at few tens to few hundreds MeV, if the shock is in the radiatively efficient regime with  $\Gamma \sim 300$  and  $R \sim 10^{12}$  cm.

### 3.2. Internal shocks in pair-dominated outflows

This case can be readily obtained from the baryon-dominated case by replacing  $m_p$  with  $m_e$ . We obtain

$$T_{\text{cool}}^{(e^\pm)} \simeq 5.9 \times 10^8 L_{52}^{-1/2} \Gamma_2 \Gamma_i^{-3} R_{12} \hat{\epsilon}_B^{-1} \hat{\epsilon}_e^{-1}. \quad (19)$$

Thus, internal shocks in the  $e^\pm$ -dominated ejecta have a very long radiative cooling time and, hence, are radiatively inefficient in our language. The peak of the synchrotron radiation in the observers frame is

$$\nu_{syn} \simeq 0.12 \text{ keV } L_{52}^{1/2} R_{12}^{-1} \Gamma_i^3 \hat{\epsilon}_B^{1/2} \hat{\epsilon}_e^2. \quad (20)$$

### 3.3. External shocks of afterglows

In the post-shock region of an external shock propagating into an external medium of density  $n_{\text{ext}}$ , we have

$$n' = 4\Gamma n_{\text{ext}} = (400 \text{ cm}^{-3}) \Gamma_2 n_{\text{ext}}, \quad (21)$$

$$\gamma_e = (m_p/m_e) \Gamma \hat{\epsilon}_e = 1.8 \times 10^5 \Gamma_2 \hat{\epsilon}_e, \quad (22)$$

$$B' = (8\pi \Gamma m_p c^2 n' \hat{\epsilon}_B)^{1/2} \simeq (39 \text{ G}) \Gamma_2 n_{\text{ext}}^{1/2} \hat{\epsilon}_B^{1/2}, \quad (23)$$

Using these quantities, we estimate the cooling time as

$$T_{\text{cool}}^{\text{AG}} \simeq 7.3 \times 10^3 \Gamma_2^{-3} n_{\text{ext}}^{-1/2} \hat{\epsilon}_B^{-1} \hat{\epsilon}_e^{-1}. \quad (24)$$

This relation is plotted in figure 4 for a very dense external medium,  $n_{\text{ext}} \sim 100 \text{ cm}^{-3}$ . Even for such an extreme case, the external shock is radiative only for very large Lorentz factors  $\Gamma \gtrsim 500$ . It is an order of magnitude larger for a more conventional value of  $n_{\text{ext}} \sim 1 \text{ cm}^{-3}$ .

We now consider two models of the external medium density profile, namely the constant density interstellar medium (ISM) and the wind outflow models.

In the *ISM model*, the Lorentz factor of a blast wave depends on the observed time as (Granot *et al* 1999)

$$\Gamma \simeq 350 E_{53}^{1/8} n_{\text{ISM}}^{-1/8} (1+z)^{3/8} t^{-3/8}, \quad (25)$$

where  $E \simeq Lt_{\text{GRB}}$  is the isotropic energy equivalent of the blast wave,  $t_{\text{GRB}}$  is the duration of a GRB and  $n_{\text{ext}} = n_{\text{ISM}} = \text{const}$  is the external medium density. In this model, the cooling time is

$$T_{\text{cool}}^{\text{AG,ISM}} \simeq 180 E_{53}^{-3/8} n_{\text{ISM}}^{-1/8} (1+z)^{-9/8} \hat{\epsilon}_B^{-1} \hat{\epsilon}_e^{-1} t^{9/8}. \quad (26)$$

In the *Wind model*, the blast wave is propagating in the wind environment with the density decreasing with distance as  $n \propto R^{-2}$ ; the Lorentz factor of the blast wave and wind density are (Chevalier & Li 2000)

$$\Gamma \simeq 270 E_{53}^{1/2} A_*^{-1/4} (1+z)^{1/4} t^{-1/4}, \quad (27)$$

$$n_{\text{ext}} \simeq (1.1 \times 10^5 \text{ cm}^{-3}) E_{53}^{-1} A_*^2 (1+z) t^{-1}, \quad (28)$$

where  $A_* = [\dot{M}_W / (10^{-5} M_\odot \text{ yr}^{-1})] / [V_W / (10^3 \text{ km s}^{-1})]$  is the wind parameter,  $\dot{M}_W$  is the mass loss rate,  $V_W$  is the wind velocity. The cooling time is

$$T_{\text{cool}}^{\text{AG,W}} \simeq 1.2 E_{53}^{-1} A_*^{-1/4} (1+z)^{-5/4} \hat{\epsilon}_B^{-1} \hat{\epsilon}_e^{-1} t^{5/4}. \quad (29)$$

In figure 5, we plot  $T_{\text{cool}}$  in the external shock versus time after the burst for both models and for two sets of afterglow parameters. We see that, except for the very early times, in both models, the emission from external shocks should be coming from far downstream, not from the main shock compression region. However, in the Wind model, the external shock can be radiative up to  $\sim 100$  s after the burst, whereas for the ISM model, the radiative shock regime can occur only at times earlier than a second after the explosion. Since the afterglow usually sets in at least several tens of seconds after the explosion, we conclude that only very early afterglow emission can, in principle, come from radiative shocks and only in the Wind model.

#### 4. Discussion

We compared the electron cooling time to the dynamical microscopic time (the plasma time,  $\omega_p^{-1}$ ) for the internal shocks in both electron-positron and baryon-dominated relativistic GRB outflows and for the external afterglow shock. We used the most recent PIC simulations to obtain  $\epsilon_e$ ,  $\epsilon_B$  and the size of the region with strong magnetic field. We evaluated and used in our analysis the emission-weighted  $\hat{\epsilon}_B$ , instead of the conventional volume-averaged quantity (for  $\epsilon_e$  both emission- and volume-averaged quantities are expected to be similar). We then evaluated the residence time of an electron in the high-field region as the size of this region over the flow speed. Thus, we did not account for clumpiness and less-than-unity filling factor of magnetic inhomogeneities (which is decreasing the effective residence time) and the electron trapping in high-field clumps (which is increasing the effective residence time). Using PIC simulations, one can study the radiative cooling effects much more accurately.

We obtained that if  $T_{\text{cool}} = t_{\text{cool}}\omega_p < (100 - 300)$ , an electron has enough time to radiate away energy comparable to its initial energy,  $\sim \gamma_e m_e c^2$ . If  $(10 - 50) < T_{\text{cool}} < (100 - 300)$ , much radiation is emitted from the strong field region at the shock jump. Therefore, we call this regime the “radiative shock” regime. If  $T_{\text{cool}} \lesssim (10 - 50)$ , the electron cooling is extremely fast and strong radiative losses are expected in the upstream region as well; hence we refer to it as the “strong cooling regime”. Note that in both these cases, Fermi acceleration of electrons is hardly possible because the electrons lose their energy every time they cross the shock. Therefore, we expect that the electron distribution will not be a power-law and, hence, a hard non-thermal tail in the radiation spectrum is hardly produced. If  $T_{\text{cool}} \gg 300$ , radiation from the shock (if any) will be coming from the far downstream region. This region has not been fully analyzed in simulations, so it is too early to draw any firm conclusions about this regime. However, if we extrapolate the decay rate  $\epsilon_B \propto 1/d$  ( $d$  is the distance from the shock front) as seen in PIC  $e^\pm$  simulations, then the shocks in this regime should be very weakly radiative.

The obtained results are as follows. For internal shocks in  $e^\pm$ -pair-dominated outflows, the cooling time exceeds the microphysics time by many orders of magnitude,  $T_{\text{cool}} \gg 300$  for the entire range of reasonable shock and outflow parameters. Therefore, emission from such pair-dominated shocks will have to be produced (if at all) in the far downstream region, not at the shock front.

Somewhat similar conclusions follow for the external afterglow shocks in the electron-proton plasma. For most of the blast wave conditions, these shocks are also in the weakly radiative regime. The observed afterglow emission has to be produced in the large volume of the downstream region. The emission from the high-field region at the shock jump is strong for ultra-relativistic shocks with  $\Gamma \gtrsim 350$  in a high-density external medium,  $n_{\text{ext}} \sim 100 \text{ cm}^{-3}$ , and for even higher  $\Gamma$ 's at lower densities. Figure 4 shows  $T_{\text{cool}}$  as a function of  $\Gamma$ . Dark and light blue regions indicate the range of  $\Gamma$  for which an external shock is in the radiative regime.

The cooling time for the ISM and Wind models of the ambient density profile as a function of time after the burst is shown in figure 5. We obtained that, except for the very early times, the shocks (in both models) are characterized by very large  $T_{\text{cool}}$ , indicating that the observed emission should be produced in the far downstream region. In the ISM model, the shock can be radiative only at the very early times, earlier than a second after the burst. In contrast, the shock in the Wind model can be in the radiative regime until about a hundred seconds after the explosion. Usually, the



afterglow sets in at least a few tens of seconds after the explosion. Therefore, there is a chance that the very early afterglow emission from a shock in the Wind medium is produced at the shock front itself. We speculate that one can expect a break in the afterglow (steepening of the light-curve) at about 10 to 100 seconds, indicating the transition from the radiatively efficient to the radiatively inefficient shock. It is likely, though, that this early afterglow emission will be swamped in a brighter prompt or high-latitude emission. It is far too early to make quantitative predictions, however, because radiative cooling can change the shock formation and evolution on a microscopic scale. A further study requires a radiative PIC simulation. It is quite possible that magnetic fields may be produced by the relativistic Richtmyer-Meshkov instability (the vorticity-generating fluid instability, Sironi & Goodman 2007; Goodman & MacFadyen 2007; Milosavljevic *et al* 2007) in the afterglow phase. The dependence  $\epsilon_B \propto \Gamma^{-1}$  can be a benchmark of the model.

The most remarkable results are obtained for internal shocks in the baryon-dominated scenario. The “diagrams of state” – the contours of constant  $T_{\text{cool}}$  in the planes  $R$ - $\Gamma$  and  $R$ - $\Gamma_i$  are shown in figures 2, 3. One can see that the regime of *strong cooling* is limited to low bulk Lorentz factors,  $\Gamma \lesssim 60$  and small radii  $R \lesssim 10^{10} - 10^{11}$  cm. Such shocks are well below the photosphere, located at  $R_{\text{ph}} \sim 10^{14} - 10^{15}$  cm for such low  $\Gamma$ 's, which makes them hardly observable. However, *radiative shocks* with  $T_{\text{cool}} \sim 100 - 300$  can form above the photosphere for the conventionally assumed GRB parameters,  $\Gamma \sim 200 - 300$ ,  $L \sim 10^{52}$  erg/s,  $\Gamma_i \gtrsim 2.5$ , as is seen from figure 3. In this figure, we considered shocks forming at the photospheric radius, i.e., when  $R_i = R_0(2\Gamma^2) \simeq R_{\text{ph}}$ . One should keep in mind that internal shocks can occur at radii smaller than  $R_i$  if the outflow modulation occurs due to instabilities in the outflow/jet itself, at radii  $R \gg R_0$  where the flow is already ultra-relativistic, rather than at the base of the jet, at  $R \sim R_0$  (Rees & Mészáros 2005). This substantially relaxes the conditions on the optical depth, especially at high  $\Gamma$ . Note that depending on the efficiency of conversion of the kinetic energy into radiation, the radiation from internal shocks can produce the second,  $e^\pm$ -pair photosphere. Should this happen, the optical depth is estimated to be from few to ten. One can expect, therefore, the appearance of a thermal component in the spectrum. Such optical depths are, nevertheless, not enough to completely smear out a non-thermal component;  $\tau_\pm$  greater than a hundred are likely needed for this (Pe’er & Waxman 2004). The pair opacity is less of a problem for low-energy GRBs: for  $L \sim 10^{48} - 10^{49}$  erg/s,  $\Gamma \sim 200$  and the radiation efficiency of about 10%, the radiative shocks can occur at  $\tau_\pm \sim 1$  and well above the baryonic photosphere.

The existence of the regime of GRBs with strong radiative cooling has many interesting implications.

The first of them concerns radiation emitted at such shocks. The magnetic fields at the shock front are highly inhomogeneous and anisotropic on very small scales, much smaller than the typical electron gyro-radius. The fields predominantly have the filamentary structure, reminiscent of the filaments of the Weibel instability undergone subsequent numerous mergers in the foreshock region (see, e.g., Spitkovsky 2008; Chang *et al* 2008). It has been predicted that radiation produced in such small-scale fields (called the “jitter radiation”) should be spectrally different from the conventional synchrotron radiation (Medvedev 2000). The steeper than synchrotron low-energy spectral slope,  $F_\nu \propto \nu^1$ , was an attractive solution to the “synchrotron line of death” problem in prompt GRBs (Preece *et al* 1998; Medvedev 2000). Because of the anisotropic, filamentary structure of magnetic fields at the shock front, jitter

radiation is predicted to be anisotropic too, with its spectral shape varying with angle between the shock normal and the line of sight (Medvedev 2006). Combined with relativistic kinematics, the model reproduces certain spectral correlations observed in the time-resolved analysis of GRB data (Kaneko *et al* 2006), as well as the ubiquity of flat,  $F_\nu \propto \nu^0$ , spectra in the sample (Pothapragada *et al* 2007). Afterglow lightcurves in the jitter regime have also been recently calculated (Medvedev *et al* 2007; Workman *et al* 2008).

The second one deals with the fact that realistic GRB shocks in a certain parameter regime are now accessible to simulations. Present 2D PIC simulations already resolve the shock formation and evolution, generation of magnetic fields in the foreshock region and their amplification toward the shock front, the electron acceleration to near equipartition with the protons and, tentatively, Fermi-type acceleration. The shocks in the radiative regime are remarkable in that the energetic electrons are able to radiate a substantial fraction of the shock energy, thus making the shocks radiatively efficient and, hence, observable as prompt GRBs. This opens the possibility to ultimately understand the properties of collisionless relativistic shocks. Moreover, by adding radiative cooling in the PIC simulations, one can study to what extent rapid cooling of electrons affects the shock structure on the microscopic scale. At last, one can obtain the radiation spectra directly from PIC simulations (this possibility has already been demonstrated by Hededal 2005), compare them with observational data and, after all, confirm or falsify the jitter model of prompt GRBs. All this does not seem feasible at present, however, for the shocks in the weakly radiative regime, in which the structure and dynamics of the magnetic field far behind the shock is crucial, but which is still difficult to trace with available computational resources.

Third, in the radiatively efficient regime, an electron loses its energy every time it is crossing the shock, so Fermi acceleration of the electrons will be quite inefficient. One can expect that a power-law electron distribution will not form in this case and, as a consequence, the observed radiation spectrum may not have an extended non-thermal tail. Moreover, the peak of the emitted radiation is predicted for such a regime to be in the multi-MeV range, where the comptonized component is conventionally expected, but no strong second peak is expected in the keV-MeV range. This prediction can soon be tested with *Fermi* (former *GLAST*) observatory.

Finally, the Weibel instability and radiation production in conditions very close to those in GRBs can be studied in existing laboratory experiments. The generation of filamentary magnetic fields, indicative of the Weibel instability, has been demonstrated in numerous laser-produced plasma experiments (see, e.g., Tatarakis *et al* 2003). In these experiments, a Petawatt laser beam with the intensity  $I \sim 10^{20} - 10^{22} \text{ W cm}^{-2}$  produces a relativistic plasma of density  $n \sim 10^{19} - 10^{21} \text{ cm}^{-3}$  and relativistic electrons with the Lorentz factor of one to few hundred. Because the the density in the experiments is so close to the density in internal shocks,  $\sim 10^{16} \text{ cm}^{-3}$ , the plasma skin depths differ by about two orders of magnitude, cf.,  $c/\omega_{pp} \sim 10 \mu\text{m}$  in the lab and  $\sim \text{few mm}$  in prompt GRBs. For the typical transverse size of a laser beam of  $\sim 100 \mu\text{m}$ , a large number of the Weibel filaments are produced in the target, which makes the further study of the nonlinear dynamics of filaments feasible. By launching a probe relativistic electron beam through the target and performing the X-ray and beam diagnostics, as is proposed in the *Hercules* experiment¶, one can directly and

¶ <http://www.eecs.umich.edu/CUOS/research/index.html>

simultaneously probe the magnetic field structure and the spectral properties of the emitted radiation. These experiments can be done in a number of existing laser facilities, such as *Vulcan*, *Hercules*, *Omega*, *NIF* and a few other. Apart from being a very exciting possibility for the *Laboratory Plasma Astrophysics*, such experimental studies are crucial for the verification of numerical results.

In this paper, we evaluated the cooling time in GRBs with reasonable accuracy. One should understand, however, that there are intrinsic uncertainties in the values of certain parameters, which are difficult to quantify. In our calculation of the average residence time of an electron in a region of high magnetic field at the shock front, we did not take into account the effective filling factor of the field, nor did we consider the increase of the residence time due to the electron trapping. Such effects strongly depend on individual particle trajectories and are, therefore, sensitive to both the field structure and the particle distribution function. We, however, evaluated and included the effect of the clumpiness of the magnetic field on the effective (emission-weighted)  $\hat{\epsilon}_B$ , as it is relatively straightforward. Here we also used the results of 2D simulations, which may differ from a realistic 3D case. More importantly, in the strong cooling regime, the electron cooling occurs on the time-scale of the shock formation. This effect can, in principle, change the entire shock structure. Since the effect of radiative cooling has never been studied before, the results of this paper are suggestive. How does strong electron cooling change the collisionless shock formation, its structure and dynamics? The answer to this question can be obtained from future numerical PIC simulations which include radiative effects. However, we can speculate that shocks with strong electron cooling will likely have longer transition regions than the non-radiative shocks. This is because electron heating is an integral part of the electron-ion shocks (Spitkovsky 2008), as it enables electrons to escape the ion filaments. This reduces filament shielding, and facilitates ion filament merging, which leads to shock formation. If electrons are kept cold in the upstream, the shock may thus take longer to form (Lyubarsky & Eichler 2007; Gedalin *et al* 2008). Finally, in our study we completely ignored the magnetic fields present in the upstream region. These fields are relatively weak, compared to the fields at the shock itself, but they can make a non-negligible contribution to the electron cooling if they occupy a large volume. Simulations of electron-positron shocks indicate that even in the longest simulations the upstream magnetic field has not reached a steady state, but continues to grow with the simulation time (Keshet *et al* 2008). In our analysis we also ignored the presence of the fields in the downstream, which have also been demonstrated to be affected by the upstream fields. Thus, our analysis is quite conservative since both the upstream and downstream fields can only decrease the electron cooling time and/or increase the radiative efficiency of the shock.

### Acknowledgments

This work has been supported by NSF grants AST-0708213, AST-0807381, NASA ATFP grant NNX-08AL39G, Swift Guest Investigator grant NNX-07AJ50G and DOE grant DE-FG02-07ER54940. A.S. acknowledges the support from Alfred P. Sloan Foundation fellowship.

### References

Chang, P., Spitkovsky, A., & Arons, J. 2008, *Astrophys. J.*, 674, 378

- Couch, S. M, Milosavljevic, M., & Nakar, E. 2008, arXiv:0807.4117
- Chevalier, R. A., & Li, Z.-Y. 2000, *Astrophys. J.*, 536, 195
- Gedalin, M., Balikhin, M. A. & Eichler D. 2008, Phys. Rev. E, 77, 026403
- Goodman, J., & MacFadyen, A. I. 2007, ArXiv e-prints, arXiv:0706.1818
- Granot, J., Piran, T., & Sari, R. 1999, *Astrophys. J.*, 527, 236
- Hededal, C. B. 2005, PhD thesis; arXiv:astro-ph/0506559
- Huntington, C., et al. 2008, Bull. AAS, 40, 192
- Kaneko, Y., Preece, R. D., Briggs, M. S., Paciesas, W. S., Meegan, C. A., & Band, D. L. 2006, *Astrophys. J. Suppl.*, 166, 298
- Katz, B., Keshet, U., Waxman, E. 2007, *Astrophys. J.*, 655, 375
- Keshet, U., Katz, B., Spitkovsky, A., & Waxman, E. 2008, ArXiv e-prints, 802, arXiv:0802.3217
- Kobayashi, S., Piran, T., & Sari, R. 1997, *Astrophys. J.*, 490, 92
- Lyubarsky Y. & Eichler D. 2007, *Astrophys. J.*, 647, 1250
- Maksimchuk, A., et al. 2008, Phys. Plasmas, 15, 056703
- Medvedev, M. V., & Loeb, A. 1999, *Astrophys. J.*, 526, 697
- Medvedev, M. V. 2000, *Astrophys. J.*, 540, 704
- Medvedev, M. V. 2006, *Astrophys. J.*, 637, 869
- Medvedev, M. V., Lazzati, D., Morsony, B. C., & Workman, J. C. 2007, *Astrophys. J.*, 666, 339
- Mészáros, P. & Rees, M. J. 2000, *Astrophys. J.*, 530, 292
- Meszáros P. 2006, Rep. Prog. Phys., 69, 2259
- Milosavljevic, M., Nakar, E., & Zhang, F. 2007, ArXiv e-prints, 708, arXiv:0708.1588
- Pe'er, A. & Waxman, E. 2004, *Astrophys. J.*, 613, 448
- Preece, R. D., Briggs, M. S., Mallozzi, R. S., Pendleton, G. N., Paciesas, W. S., & Band, D. L. 1998, *Astrophys. J. Lett.*, 506, L23
- Pothapragada, S., Reynolds, S., Graham, S., & Medvedev, M. V. 2007, APS Meeting Abstracts, 1007
- Rees, M. J., & Mészáros, P. 2005, *Astrophys. J.*, 628, 847
- Reynolds, S., Pothapragada, S., & Medvedev, M. 2006, APS Meeting Abstracts, 1080P
- Reynolds, S., Pothapragada, S., Graham, S., & Medvedev, M. V. 2007, APS Meeting Abstracts, 1021
- Sironi, L., & Goodman, J. 2007, *Astrophys. J.*, 671, 1858
- Spitkovsky, A. 2008, *Astrophys. J. Lett.*, 673, L39
- Tatarakis, M., et al 2003, *Phys. Rev. Lett.*, 90, 175001
- Workman, J. C., Morsony, B. J., Lazzati, D., & Medvedev, M. V. 2008, *Mon. Not. R. Astron. Soc.*, 386, 199

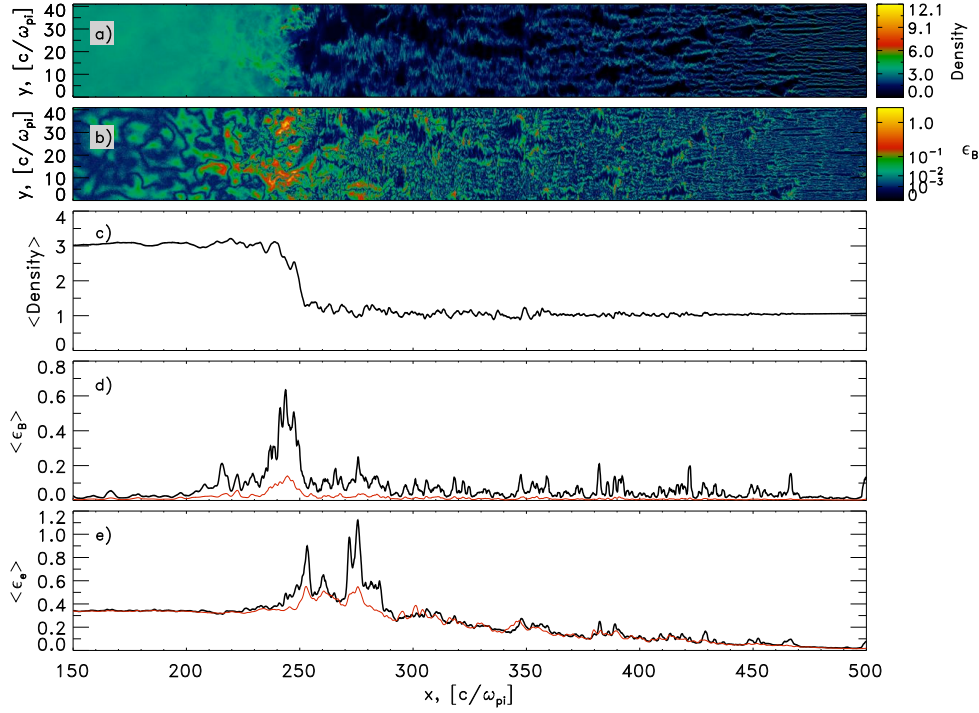


**Figure 1.** A snapshot of a shock from PIC simulation with  $\Gamma = 15$  and  $m_i/m_e = 100$ . (a) and (b) — Maps of the particle density  $n$  and the normalized magnetic field strength  $\epsilon_B$ , respectively. The incoming flow moves from right to left, while the shock propagates to the right. The simulation is performed in the downstream frame. (c) — Density profile averaged over the transverse ( $y$ ) direction. (d) and (e) — The  $y$ -averaged profiles of  $\epsilon_B$  and  $\epsilon_e$  (red curves) and the “emission-weighted” profiles of  $\hat{\epsilon}_B$  and  $\hat{\epsilon}_e$  (black curves) respectively.

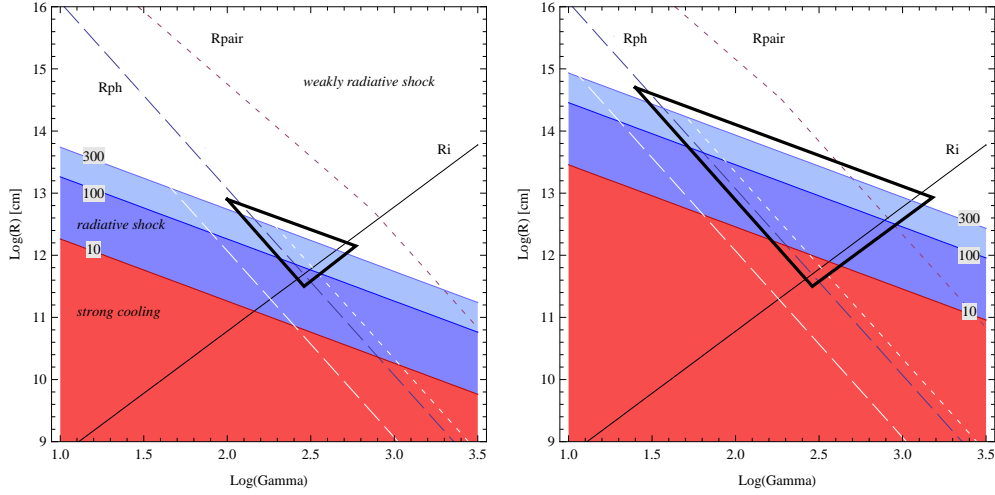


**Figure 2.** Contours of  $T_{\text{cool}}$  vs.  $\Gamma$  for  $\Gamma_i = 4$  (left panel) and a somewhat unrealistically high  $\Gamma_i = 10$  (right panel) for the internal shocks in baryon-dominated outflows for  $T_{\text{cool}} = 10, 100, 300$ . Red filled regions correspond to  $T_{\text{cool}} < 10$  (the “strong cooling” regime), dark and light blue regions correspond to  $10 < T_{\text{cool}} < 100$  and  $100 < T_{\text{cool}} < 300$ , respectively (the “radiative shock” regime), and the white region corresponds to the “weakly radiative shock” ( $T_{\text{cool}} > 300$ ). The black triangle outlines the range of parameters where radiative shocks occur and may be observable. In all cases,  $L_{52} = 1$ ,  $L_\gamma = 0.1L$ ,  $t_{v,-4} = 1$ . The radii,  $R_i$ ,  $R_{\text{ph}}$  and  $R_{\text{pair}}$  are plotted for reference. Internal shocks can occur above  $R_i$  line; optical depths,  $\tau_b$  and  $\tau_\pm$ , are less than unity above lines  $R_{\text{ph}}$  and  $R_{\text{pair}}$ , respectively. White lines in the left panel denote radii at which the optical depths  $\tau_b$  and  $\tau_\pm$  are equal to 10 (dashed and dotted lines respectively). It is expected that some non-thermal spectral signatures of radiation emitted from not so large optical depths of  $\tau \lesssim 10$  may still be observable in addition to the strong thermal component.

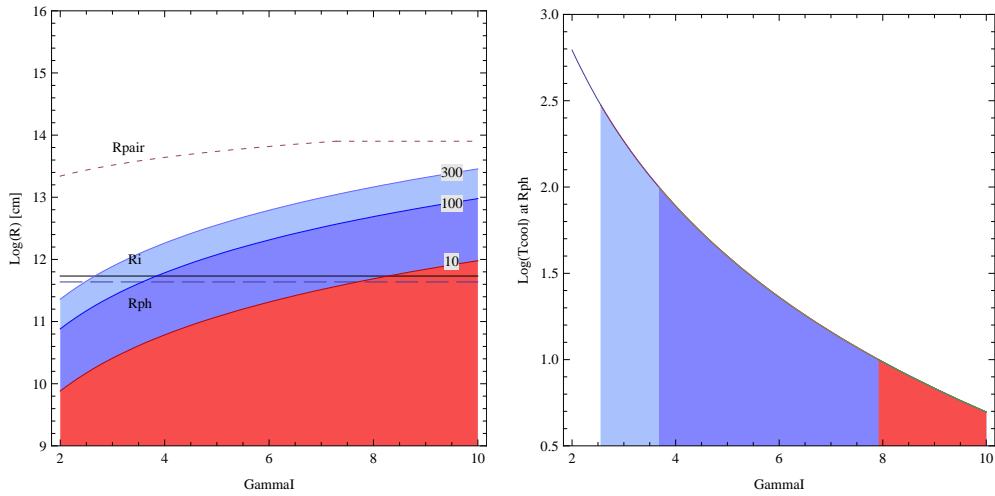


**Figure 3.** (left panel) Contours of  $T_{\text{cool}}$  vs. the Lorentz factor of internal shocks,  $\Gamma_i$ , for the internal shocks in the  $\Gamma = 300$  ejecta. (right panel) Dimensionless cooling time,  $T_{\text{cool}}$ , in internal shocks at the baryonic photosphere vs.  $\Gamma_i$ . Color coding and the outflow parameters are the same as in figure 2.

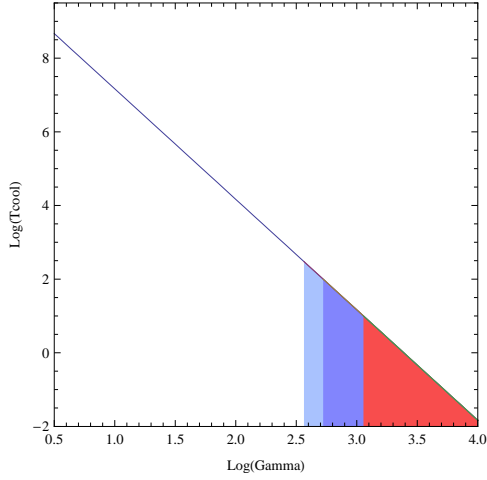


**Figure 4.** Cooling time in afterglows vs. the outflow Lorentz factor, for  $n_{\text{ext}} = 100 \text{ cm}^{-3}$ . Color coding and the outflow parameters are the same as in figure 2.

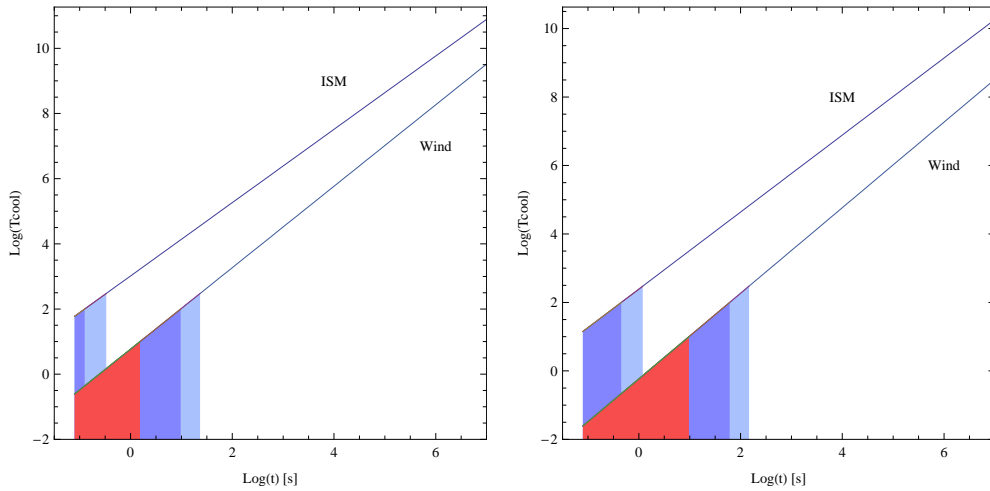


**Figure 5.** Cooling time in afterglows vs. time after the burst, for the ISM and Wind models of the external density. In the left panel, we use the “typical” parameters  $E = 10^{53} \text{ erg}$ ,  $A_* = 1$  and  $n_{\text{ISM}} = 1 \text{ cm}^{-3}$ , whereas in the right panel, we use a rather extreme set of parameters,  $E = 10^{54} \text{ erg}$ ,  $A_* = 10$  and  $n_{\text{ISM}} = 100 \text{ cm}^{-3}$ . In both cases, we put a GRB at a typical  $z = 2$ ; time in the plots ranges from 0.1 s to 100 days. Color coding is the same as in figure 2.